Fluid Dynamics & Materials Processing

Tech Science Press

DOI: 10.32604/fdmp.2022.018526

ARTICLE

Influence of Particle Size Distribution on the Optical Properties of Fine-Dispersed Suspensions

Dmitrii Kuzmenkov[1,*], Pavel Struchalin[1,2], Yulia Litvintsova[1], Maksim Delov[1], Vladimir Skrytnyy[1] and Kirill Kutsenko[1]

[1]National Research Nuclear University MEPhI (Moscow Engineering Physics Institute), Moscow, 115409, Russian Federation

[2]Western Norway University of Applied Sciences, Bergen, 5063, Norway

[*]Corresponding Author: Dmitrii Kuzmenkov. Email: dmkuzmenkov@mephi.ru

Received: 30 July 2021 Accepted: 04 September 2021

ABSTRACT

Nanofluids have great potential for solar energy harvesting due to their suitable optical and thermophysical properties. One of the promising applications of nanofluids is utilization in solar collectors with the direct absorption of light (DASC). The design of a DASC requires detailed knowledge of the optical properties of nanofluids, which can be significantly affected by the particle size distribution. The paper presents the method to take into account the particle size distribution when calculating nanofluid extinction spectra. To validate the proposed model, the particle size distribution and spectral absorbance were measured for aqueous suspension with multi-walled graphite nanotubes; the minimum size of primary nanoparticles was 49 nm. The proposed model is compared with experiments demonstrating the concentration averaged and maximum discrepancies of 6.6% and 32.2% against 12.6% and 77.7% for a model assuming a monosized suspension.

KEYWORDS

Nanoparticles; multi-walled carbon nanotubes; fine-dispersed suspension; optical properties

Nomenclature

ABS	Spectral absorbance
a_i, b_i	Coefficients of scattered electromagnetic field
C_{ext}	Extinction cross-section, m^2
d_p	Diameter of particle or particle agglomerate, m
F	Volume fraction of particles having the size of $d_{p,i}$ to the total volume of particles
f_v	Particle volume fraction
l	Thickness of the suspension sample
m	Complex refractive index of the particles relative to the base fluid
n	Real part of the complex refractive index of the base fluid

Greek symbols

α	Size parameter of particle
λ	Wavelength, m
Π	Number of particles per unit volume of the base fluid, m^{-3}

σ	Extinction coefficient, m^{-1}
χ	Wave number, m^{-1}

Subscripts

p	Particle
bf	Base fluid
nf	Nanofluid; fine-dispersed suspension

Abbreviations

DASC	Direct Absorption Solar Collector
MWCNT	Multi-walled Carbon Nanotubes
PSD	Particle Size Distribution

1 Introduction

The last few decades have been characterized by an ever-growing interest of the world community in renewable energy, particularly solar energy, as one of the most promising renewable energy sources [1]. Currently, solar energy is used to generate electricity and heat, both on an industrial scale and within individual households [2–4].

Several devices have been developed to convert solar radiation energy into thermal energy—the so-called solar collectors. They differ structurally, but the general principle of operation is to transfer thermal energy from a blackened receiver, heated by solar radiation, to the coolant. The blackened surfaces of the volumes inside which the coolant flows or the outer surfaces of the tubes through which the coolant flows can be used as a receiver. The disadvantage of such systems is an overheated outer surface, which loses a significant part of the received energy into the environment. New designs of such devices and different ways to enhance the efficiency of existing technical solutions are proposed [5–8]. One such solution uses a nanofluid (a stable suspension consisting of a base fluid and nano-sized solid particles dispersed in it) or fine-dispersed suspensions. The nanofluids show improved heat transfer [9–17] and optical properties [18–21] than traditional single-phase heat transfer fluids and demonstrate high potential for solar energy applications [20,21]. Moreover, the nanofluids and nanoparticle suspensions have found multiple applications in microelectronics [16,17,22–24], nuclear power generation [25], medicine [26,27], chemical technology [28], etc.

The use of nanofluids allows one to change the absorption mechanism of solar energy, namely, to carry out solar energy absorption in the coolant itself, flowing in a transparent volume or channels. As a result, the temperature of the outer surface of the receiver significantly decreases, and, accordingly, the heat losses to the environment reduce.

The ability of a nanofluid to absorb solar energy directly depends on the concentration of particles and their properties—shape, size, and distribution [29–33]. Studies have shown that one can choose the optimal concentration of particles that provide the best absorption of radiant energy [34–36]. However, its value in each specific case may be different and depend on the optical properties of the manufactured nanofluid, which, in turn, depend on its composition and particle characteristics [37,38].

The absorbance of light energy by nanofluid can be determined experimentally. However, the development of a model that allows one to determine the optical properties of nanofluids based on their composition and taking into account the particle size distribution would make it possible to reduce the number of routine experiments and the need for the availability and use of expensive equipment. Such a model can also find application in the calculation of a designed solar collector with nanofluid. Of

particular interest is the prediction of changes in the performances of the solar collector with time during the deposition of particles, changes in the fraction of particles, and their size distribution.

Several papers [39–42] propose the method or model to calculate the optical properties of nanofluids based on Rayleigh or Mie scattering theories. For example, Sharaf et al. [39] proposed the optical model based on Rayleigh scattering theory coupled with hybrid Eulerian-Lagrangian treatment for simulating heat and mass transfer in the nanofluid. Their results showed that particle spatial distribution could significantly affect the absorption properties of nanofluid and the efficiency of the nanofluid-based solar collector. In [39,42], the model for calculating the extinction coefficient of nanofluids was used to determine the volumetric heat generation, which was then imported in CFD simulation of the heating and evaporation of nanofluids. Both studies pointed out the efficiency of heating and evaporation of nanofluids are significantly affected by the average size of particles (or particle agglomerates) and particle fraction. However, in these works, the optical properties of nanofluids were determined using the effective average particle size, i.e., under the assumption of monodispersity of the studied nanofluid, although this assumption cannot always be ensured in practice, especially during the long-term operation of the nanofluid.

Song et al. [43] studied the absorption spectra of the water-based nanofluid with TiO_2 nanoparticles taking into account particle size distribution obtained by the population balance model. Comparing the results of modeling with the experimental data, they have shown that considering PSD can play a significant role when calculating the extinction spectra of the nanofluid. Thus, according to Song et al. [43], the discrepancies between the conventional monodisperse model and experimental data are more than 90% discrepancies. Furthermore, considering PSD improves the accuracy of calculating the absorption coefficient significantly. Moreover, Song et al. [43] note that the influence of particle size distribution on the absorption spectra of the nanofluid grows with increasing particle fraction. Thus, the results by Song et al. [43] confirm the necessity of considering PSD when calculating the spectral optical properties of the nanofluid. However, the optical model by Song et al. [43] is based on Rayleigh scattering theory and Fraunhofer diffraction theory, which are not applicable when the particle diameter is comparable in size with the wavelength of the incident radiation. Moreover, the nanofluid composition studied by Song et al. [43] is hardly applicable to solar collectors due to instability in the absence of surfactants.

The present paper aims to develop a method to consider particle size distribution (PSD) when calculating the optical properties (extinction coefficient, spectral absorbance) of the suspensions. The proposed model is validated against the experimental data and conventional model for monodispersed suspension.

2 Materials and Methods

2.1 Model Description

The model to determine extinction spectra of the fine-dispersed suspension, taking into account particle distribution, consists of two main parts. First, using the conventional approach based on Mie scattering theory, we determine the extinction spectra of the nanofluid of known composition as a function of particle diameter. The optical properties required for calculations, namely real and imaginary parts of the complex refractive index, can be found elsewhere [44,45]. Second, the derived expression for extinction spectra is averaged over volumetric particle size distribution, obtained via experimental measurement.

According to Mie scattering theory, the extinction cross-section of an individual spherical particle appears as [46]:

$$C_{ext} = \frac{2\pi}{|\chi|^2}\sum_{i=1}^{\infty}(2i+1)\mathrm{Re}[a_i + b_i], \tag{1}$$

where $\chi = 2\pi n/\lambda$ is a wave number; λ is a wavelength; n is a real part of the complex refractive index of the base fluid. In Eq. (1), a_i and b_i are the coefficients of the scattered electromagnetic field, which reads as:

$$a_i = \frac{m\psi_i(m\alpha)\psi_i'(\alpha) - \psi_i(\alpha)\psi_i'(m\alpha)}{m\psi_i(m\alpha)\zeta_i'(\alpha) - \zeta_i(\alpha)\psi_i'(m\alpha)}; \tag{2}$$

$$b_i = \frac{\psi_i(m\alpha)\psi_i'(\alpha) - m\psi_i(\alpha)\psi_i'(m\alpha)}{\psi_i(m\alpha)\zeta_i'(\alpha) - m\zeta_i(\alpha)\psi_i'(m\alpha)}, \tag{3}$$

where m is a complex refractive index of the particles relative to the base fluid; $\alpha = \pi n D_p/\lambda$ is the size parameter of particle; $\psi_i(z)$ and $\zeta_i(z)$ are Riccati-Bessel functions of i-th order. Ricatti-Bessel functions can be expressed through the Bessel functions of the first (J_ν) and second (Y_ν) kind: $\psi_i(z) = \sqrt{\pi z/2}J_{i+1/2}(z)$ and $\zeta_i(z) = \sqrt{\pi z/2}\left(J_{i+1/2}(z) + Y_{i+1/2}(z)\right)$.

The infinite series in Eq. (1) cannot be calculated numerically. However, a maximum index n_{max}, which defines the upper summation limit, can be used to overcome this limitation. Hota et al. [41] proposed the following expression to estimate the maximum index:

$$n_{\max} = \left[2 + \alpha + 4\alpha^{1/3}\right], \tag{4}$$

where square brackets denote to integer part.

Once the extinction cross-section of an individual particle is computed, the extinction coefficient of particles dispersed in the base fluid can be determined following Bohren et al. [46] as:

$$\sigma_p = \Pi C_{ext}, \tag{5}$$

where Π is the number of particles per unit volume of the base fluid.

Assuming the particles are spherical and distributed in the base fluid uniformly, Π can be expressed through the volume fraction of particles f_v: $\Pi = 6f_v/(\pi D_p^3)$.

Eq. (5) does not consider the absorption into the base fluid, although the base fluid can absorb radiation strongly enough within some wavelength ranges. The absorption in the base fluid can be accounted for according to Taylor et al. [40] by summing the extinction coefficients of particles σ_p (Eq. (5)) and base fluid σ_{bf}:

$$\sigma_{nf} = \sigma_p + (1 - f_v)\sigma_{bf}. \tag{6}$$

The extinction coefficient of the base fluid can be calculated according to Bohren et al. [46] as $\sigma_{bf} = 4\pi k/\lambda$, where k is the imaginary part of the complex refractive index of the base fluid. In the current study, we use the water-based suspension with dispersed graphite nanotubes to validate the proposed model. The complex refractive indexes of water and graphite are found in works [44,45]. However, this study utilizes the complex mixture of water, ethanol, sodium dodecyl sulfate, and defoaming agent as a base fluid. Therefore, the extinction spectrum of the base fluid is determined experimentally to avoid inaccuracies when calculating extinction in a mixture of the complex composition according to reference data (Subsection 2.2).

Eq. (6) is commonly used to estimate the extinction spectra of the nanofluid. However, it does not contain any corrections that consider the particle size distribution in the nanofluid. Thus, this

expression applies only to a monodisperse suspension (hereinafter, for simplicity, we refer to Eq. (6) as a "monodisperse model").

In order to account for the particle size distribution, we propose to average the extinction coefficient over the volume fraction of particles having the size of $d_{p,i}$ to the total volume of particles in the suspension. Thus, the average extinction coefficient can be expressed as follows:

$$\overline{\sigma_{nf}} = \sum_{i=1}^{N} \sigma_{nf}\left(d_{p,i}\right) F_i, \tag{7}$$

where F_i is the volume fraction of particles having the size of $d_{p,i}$ to the total volume of particles in the suspension, which satisfies the relation $\sum_{i=1}^{N} F_i = 1$, and N is the number of particle sizes.

According to the definition of F_i, it can be expressed as $F_i = V_{p,i}/V_p$, where $V_{p,I}$ is the volume of particles having the size of $d_{p,I}$, and V_p is the total volume of particles in the suspension. Thus, the product of F_i and particle volume fraction f_v is the volume fraction of particles having the size of $d_{p,I}$ in the suspension. Therefore, the method proposed for considering particle distribution (Eq. (7)) is equivalent to that used for calculating the extinction spectra of hybrid nanofluids, composed of few types of nanoparticles [46,47]. However, in this study, the optical properties of the particles remain unchanged while the particle size varies.

Here, we should note that Eq. (7) assumes the particle size distribution discrete, although the PSD is generally a continuous function. However, the PSD obtained experimentally in this study is discrete. Therefore, to exclude possible errors associated with the interpolation of experimental data, the calculation of the suspension extinction coefficient was carried out for a discrete PSD, which was obtained directly from the experiment (Subsection 2.2).

Substituting Eqs. (1), (4), (5), and (6) into (7) and considering the relation between the extinction coefficient and spectral absorbance, the final expression for the spectral absorbance is derived:

$$\overline{ABS_{bf}} = l\overline{\sigma_{bf}}, \tag{8}$$

where l is the thickness of the suspension sample in the direction of radiation propagation.

However, in the case of a monodisperse model, the calculations should be carried out at a constant particle size determined by averaging over the volumetric particle size distribution:

$$\overline{D_p} = \sum_{i=1}^{N} d_{p,i} F_i. \tag{9}$$

The experimental measurements of particle size distribution and spectral absorbance of suspensions are described in Subsection 2.2, "Experiments".

2.2 Experiments

In this study, the multi-walled carbon nanotubes DEALTOM [48], manufactured by Research and Production Enterprise "Nanotechnology Center" (Moscow, Russia), were used for suspension preparation. The initial nanopowder consists of nanotubes mainly of two diameters: 49.3 ± 0.45 nm and 72.0 ± 0.45 nm. According to [48], the maximum length of the nanotubes is ~5 μm. The base fluid was prepared using distilled water with supplementary chemicals: 10% of ethanol, 0.1% of sodium dodecyl sulfate (SDS), and 0.2% of defoaming agent, produced by Karcher [49]. The chemicals were added to mimic a composition potentially used in a direct absorption solar collector tailored to perform in continental

climate conditions. To obtain the reference data for the proposed optical model, the absorbance of the base fluid ABS_{bf} was measured using Varian Cary 100 UV-visible spectrophotometer [50] in the wavelength range from 200 to 900 nm with an increment of 1 nm. Basing on this data, the extinction coefficient of the base fluid was calculated as $\sigma_{nf} = ABS_{bf}/l$, where l is the thickness of the sample in the direction of radiation propagation.

The suspensions were prepared by a two-stage method [39,40,42]. First, the mass of the dry powder was measured using the SF-400D Electronic Compact Scale (±10 mg). Next, the components of the suspension sample were mixed in a sealed container. Then the container was placed in an ultrasonic bath (Sapphire, 100 W, 35 kHz [51]), and its contents were dispersed for half an hour. The initial particle mass fractions of the prepared suspension samples were 0.008 and 0.02 wt%. Further analysis of the suspension samples showed that after 6–8 h of maturing, the mass fraction of particles in the suspension decreased approximately twice due to the sedimentation of particle agglomerates. The mass fraction decrease was estimated by measuring the mass of particle sediment using the mentioned scale (SF-400D Electronic Compact Scale). The error of determining the final particle concentration did not exceed ±15%.

A day after preparation, the size distribution of particles (particle agglomerates) in the nanofluids was measured by dynamic light scattering using the Malvern Zetasizer Nano analyzer [52]. For each sample, the granulometric analysis was carried out 2 times. We took every measurement no longer than 10 min after another. The measured size distributions are presented in Fig. 1.

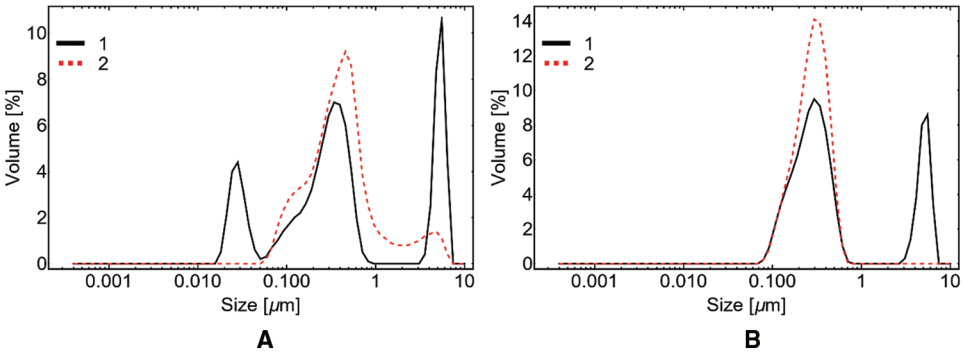

Figure 1: Particle size distributions for initial mass fractions of particles 0.008 wt% (A) and 0.02 wt% (B)

Reading Fig. 1, we should make the following comments. First, the distributions change within the studied samples, which potentially indicates the instability of the granulometric composition of nanofluids at the time of measurements. Second, as shown in Fig. 1, the PSDs exhibit a mode at 300–450 nm corresponding to the average size of the nanotube agglomerates. PSDs 1 and 2 in Fig. 1A and PSD 1 in Fig. 2B reveal modes at ~5 μm. This can be explained by the presence of air bubbles and airborne contaminants, the characteristic size of which is approximately 5 μm [53]. The magnitude of air-induced modes is greater than or equal to those corresponding to the nanotube agglomerates, explained by the low particle fractions. Thus, the air-induced mode of PSD 1 for particle fraction of 0.008 wt% is higher than the agglomerate-induced mode, while the same modes for particle fraction of 0.02 wt% are approximately equal. Subsequent measurements (PSD 2 at 0.02 wt%) demonstrated a decrease in the volume fraction of air bubbles.

The PSD 1 at 0.008 wt% is three-modal, and the first mode at ~35 nm, apparently, corresponds to the minimum diameter of the primary nanotubes (~49 nm) within the instrumental uncertainty. On the other hand, the following PSD 2 in Fig. 1A does not exhibit the same mode due to the agglomeration of

nanoparticles. Moreover, the volume-averaged size of nanotube agglomerates for PSD 2 is 460 nm against 350 nm for PSD 1.

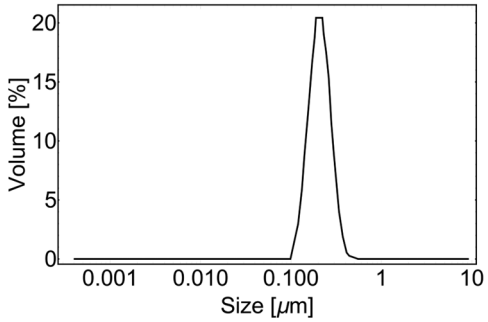

Figure 2: Result of granulometric analysis of the base fluid

As follows from the analysis of Fig. 1, increasing the particle mass fraction from 0.008 wt% to 0.02 wt% does not sufficiently affect the agglomeration process. The volume-averaged sizes of particle agglomerates are 460 and 310 nm for particle fractions of 0.008 wt% and 0.02 wt%, respectively.

A similar granulometric analysis was carried out for the base fluid. The corresponding particle size distribution is presented in Fig. 2.

As shown in Fig. 2, the distribution of the base fluid has a maximum. This maximum can be attributed to the formation of micelles due to the relatively high concentration of SDS (0.1 wt%) in the base fluid mixture [54].

The spectral absorbance of the suspension samples was measured using the same spectrophotometer (Varian Cary 100 UV-visible spectrophotometer). The measurements were carried out within the wavelength range from 200 nm to 900 nm with an increment of 1 nm. The thickness of the studied samples in the cuvette was $l = 1$ cm for all considered cases. Here, we note that all light intensity measurements were normalized by the corresponding reference intensity measurement conducted for the same empty pure cuvette. Therefore, the light reflection on the cuvette surface was accounted for by the normalization.

3 Results and Discussion

The proposed model was compared against the experimental results obtained by spectrophotometer for two initial nanoparticle mass fractions: 0.008% and 0.02%. As mentioned in Subsection 2.2 “Experiments”, the nanoparticle mass fraction in suspension reduced approximately twice after one day of maturing. Therefore, the calculations were performed at particle mass fractions of 0.004% and 0.01%. The comparison of calculations with experimental data is shown in Fig. 3.

The gray area in Fig. 3 depicts the uncertainty interval in calculating the extinction coefficient by Eq. (8) with a change in the mass concentration of particles by ±15%. The character of the experimental curve in Fig. 3B is due to the measurement limit of the spectrophotometer used. The spectrophotometer does not register radiation passed through the sample if its intensity decreases e^{10} times relative to the initial one. Thus, if the absorbance of the sample is greater than 10, then the spectrophotometer indicates the maximum allowable absorbance value within the measurement range, which is equal to 10.

The calculations by the conventional monodisperse model (green dotted line, Eq. (6)) were carried out at the volume-averaged diameter of particle agglomerates, which is determined following Eq. (9).

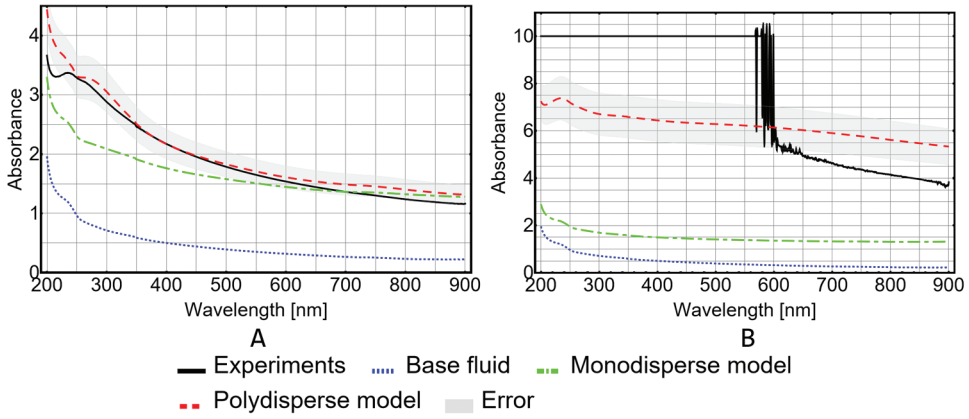

Figure 3: Spectral absorbance as a function of wavelength. Comparison of experimental data (black solid curve) with results of calculations according to Eq. (6) (green dash-dotted curve) and (7) (red dashed curve) for nanoparticle mass fraction of 0.004% (A) and 0.01% (B). The absorbance of the base fluid (blue dotted line) is plotted for reference

Considering Fig. 3, we note that account of PSD (red dashed curve) increases the accuracy of calculating the suspension extinction coefficient compared to the monodisperse model (Eq. (6)) (green dotted curve) by almost 2 times. The wavelength-averaged discrepancy relative to the experiment is 6.6% and 12.6% for polydisperse and monodisperse models, respectively, at a particle fraction of 0.004 wt%. At a particle mass fraction of 0.01%, the wavelength-averaged discrepancy for the polydisperse model is 32.2% against 77.7% for the monodisperse model. Moreover, introducing the particle size distribution into the calculation makes it possible to obtain qualitatively more correct results, which are reflected in the curves in Fig. 3. Thus, in Fig. 3, the spectral absorbance, calculated by Eq. (6), is approximately constant within the wavelength range from 600 to 900 nm. In contrast, the experiments and Eq. (7) demonstrate decreasing within the same wavelength range.

Furthermore, reading Fig. 3, we note that the addition of 0.004 wt% of MWCNT increases the absorbance by at least 87% compared to the base fluid. The minimum increase in absorbance for the suspension with 0.01 wt% of MWCNT is 410% in contrast with the base fluid. The wavelength-averaged increases in absorbance are 357% and 1740% for MWCNT fractions of 0.004 wt% and 0.01 wt%, respectively. Gimeno-Furio et al. [55] obtained similar results when studying the optical properties of water-based suspensions with single-wall carbon nanohorns. The authors reported a 665% increase in suspension absorbance within the wavelength range from 400 to 800 nm at a particle fraction of 0.002% compared to the base fluid. This increase differs from that obtained in the current study by about 200%, which can be explained by the average size of particles in the suspension sample. According to measurements in [55], the average particle size was about 100–200 nm, while, in this study, particles agglomerated up to 8 μm.

Lee et al. [56,57] also obtained similar absorbance results (extinction coefficient) for MWCNT suspensions. They experimentally investigated the extinction coefficient of water-based suspension with MWCNT and found that it varies from 4 to 12 cm^{-1} for mass fractions from about 0.004 vol% to 0.01 vol%, which is in excellent agreement with the present results. On the contrary, the extinction coefficient of water-based suspension with MWCNTs reported by Chen et al. [58] overestimates that for the present study by about 1.5 times. Primarily, this discrepancy should be attributed to the difference in MWCNT diameter, which was about 20 nm in [58]. Also, we should note that Chen et al. [58] used polyvinyl pyrrolidone as a surfactant, while in this study, we used sodium dodecyl sulfate. As shown in

contributions [29,31], the surfactant influences the optical properties of suspensions sufficiently, and in some cases, for example, at low particle fractions, this influence can be crucial.

Further, reading Fig. 3, we note that the monodisperse model underestimates the absorbance compared to the experimental data and the polydisperse model. This is due to averaging the particle size and corresponding excluding the small particles from the calculation, which better absorbs short-wave radiation. So, the average sizes of MWCNT agglomerates at mass fractions of 0.004% and 0.01% were 720 and 290 nm, respectively. Thus, the monodisperse model does not consider radiation absorption by particles of other sizes and, therefore, underestimates the absorption. The polydisperse model is free from this drawback and allows us to consider the effect of particles of all sizes on the absorption in a suspension. For a better overview of this phenomenon, we evaluate the fraction of extinction by particle agglomerates of certain sizes to the total extinction coefficient of the suspension, excluding the effect of the base fluid. This fraction η reads as:

$$\eta = \frac{\sum_i \sigma_p\left(d_{p,i}\right) F_i}{\overline{\sigma_{nf}} - (1 - f_v)\sigma_{bf}}. \tag{10}$$

Fig. 4 shows the fraction η as a function of wavelength.

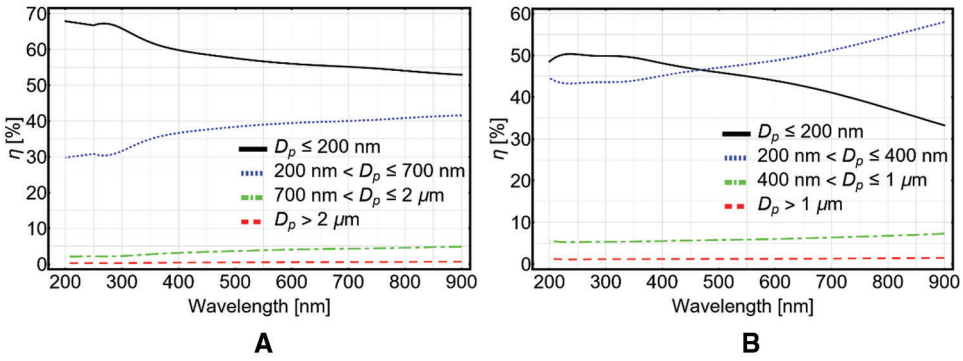

Figure 4: The fraction of extinction by particle agglomerates of certain sizes to the total extinction coefficient as a function of wavelength for particle fractions of 0.004 wt% (A) and 0.01 wt% (B)

As shown in Fig. 4A, the particle having a size below 200 nm contribute about 50–70% to the total absorbance of the suspension depending on wavelength. A slightly smaller contribution is made by agglomerates with sizes from 20 to 700 nm (30–43%). Therefore, the monodisperse model, which uses the volume-averaged diameter (720 nm), underestimates the experimental absorbance. However, this effect is depressed at high wavelengths above 600 nm, and the monodisperse model demonstrates better accuracy within this wavelength range. The influence of large MWCNT agglomerates (with diameters above 700 nm) on the absorbance is quite low for the whole considered wavelength range and does not exceed 8%. However, this is due to the low volume fraction of these agglomerates (Fig. 1A, curve "2").

Similar conclusions can be drawn by considering Fig. 4B. Here we again note the suppressing contribution of small particle agglomerates (with diameters below 400 nm) to the total absorption in the suspension, which reaches about 92%. However, the influence of agglomerates with medium sizes within the range from 400 nm to 1 μm is more considerable than Fig. 4A due to the relatively high volume fraction of such particles. On the other hand, the large particle agglomerates with sizes above 1 μm do not contribute to the absorbance since their volume fraction is meager (Fig. 1B, curve "2").

Summarizing the discussion on results in Fig. 4, we note that the largest contribution to the total extinction in the suspension is made by small particles with a size comparable to the wavelength of the incident radiation, which is in agreement with observations by Jing et al. [59].

The observed discrepancies of the model, which considers the particle size distribution (Eq. (8)), relative to experiments can be explained by several reasons. First, one of the model's key assumptions is that the particles are uniformly distributed in the base fluid, regardless of size. However, particles of different sizes are distributed in the base fluid non-uniformly due to gravity. Moreover, Azam et al. [12,16,17,28] showed that particle spatial distribution depends on temperature distribution through the thermophoresis and Brownian forces, heat source/sink rate, particle material, and chemical reactions. Therefore, the high-precise analysis of the optical properties of nanoparticle suspensions should be accompanied by modeling the heat and mass transfer. Another possible reason is dissolved gases and micelles in the base liquid, which could scatter and reflect the incident radiation resulting in a change of extinction coefficient.

The proposed model increases the accuracy of calculating optical properties of the suspension (spectral absorbance, extinction coefficient, etc.). Moreover, considering the particle size distribution when calculating the extinction coefficient allows us to obtain qualitatively more correct results, reflecting the features of the dependence of the spectral absorbance on the wavelength of the incident radiation. Furthermore, the proposed polydisperse model allows us to reveal the influence of particle size on the extinction coefficient of suspension and analyze the contribution of particles of different sizes to the total radiation absorption.

Comparing the proposed polydisperse model with the conventional one (monodisperse), we conclude that it is more suitable for numerical simulations since it can describe the contribution of particles of different sizes to the absorption of specific wavelengths. Thus, the polydisperse model provides higher accuracy in calculating the optical properties of suspensions of the complex composition and reflects the features of radiation absorption of specific wavelengths. On the contrary, the monodisperse model cannot describe the absorption features of specific wavelength ranges; however, with a proper determination of the effective particle size, the model can correctly estimate the integral absorption capacity of the suspension.

To summarize the above, the polydisperse model is suitable for calculating spectral properties such as absorption, extinction coefficient, etc. In contrast, the monodisperse fits well for determining the integral characteristics of absorption of suspensions.

4 Conclusion

The present study proposes a method to consider particle size distribution when calculating the extinction coefficient of the fine-dispersed suspensions. The proposed model is based on Mie scattering theory and uses volumetric particle size distribution, obtained using the dynamic light scattering method.

We carried out an experimental study of light extinction and granulometric analysis of water-based suspension with multi-walled carbon nanotubes for two particle fractions of 0.004 wt% and 0.01 wt%. The additional chemicals (sodium dodecyl sulfate, ethanol, and defoaming agent) were utilized to stabilize the suspension samples. The granulometric analysis performed by dynamic light scattering showed that MWCNT with the initial sizes of 49 and 72 nm aggregated in the suspension up to average sizes of 720 and 270 nm for fractions of 0.004 wt% and 0.01 wt%, respectively. The spectral absorbance measurements in the suspension samples were carried out within the wavelength range from 200 to 900 nm using a UV-visible spectrophotometer. The experimental spectral absorbance of the suspension samples was compared with the reference measurement for the base fluid, demonstrating the increase in absorbance by 357% and 1740% for particle fractions of 0.004 wt% and 0.01 wt%, respectively.

Further, we validated the proposed polydisperse model against the experimental data and conventional model, which assumes the monosized nanofluid. The polydisperse model increases the accuracy of reproducing the experimental data by about 2 times, showing the wavelength-averaged discrepancy

relative to experiments of 6.6% and 32.2% against 12.6% and 77.7% for the monodisperse model. Moreover, we analyzed the contribution of particle agglomerates of various sizes to light absorption using the proposed polydisperse model. We found that the greatest influence is due to agglomerates, the sizes of which are comparable to the wavelength of the incident radiation. Thus, the particle agglomerates with sizes below 700 nm contribute about 90% to the total absorbance in the wavelength range from 200 to 900 nm at a particle fraction of 0.004 wt%. Similarly, for the suspension with 0.01 wt% of MWCNT, the light extinction is mostly due to agglomerates with sizes below 400 nm, which contribute about 90% to the total absorbance.

All in all, the proposed polydisperse model allowed us to achieve significantly higher accuracy in reproducing experimental data than the conventional monodisperse model. A further increase in the accuracy of the proposed model is possible by considering the spatial non-uniformity of the particle distribution and coupling it with modeling the heat and mass transfer in a suspension.

Funding Statement: The reported study was funded by RFBR, Project No. 19-38-90306.

Conflicts of Interest: The authors declare that they have no conflicts of interest to report regarding the present study.

References

1. Lizunov, V., Politsinskaya, E., Malushko, E., Kindaev, A., Minin, M. (2018). Population of the world and regions as the principal energy consumer. *International Journal of Energy Economics and Policy, 8(3),* 250–257. https://www.econjournals.com/index.php/ijeep/article/view/6182.
2. Farjana, S., Huda, N., Mahmud, M. A. P., Saidur, R. (2018). Solar process heat in industrial systems: A global review. *Renewable and Sustainable Energy Reviews, 82,* 2270–2286. DOI 10.1016/j.rser.2017.08.065.
3. Herez, A., El Hage, H., Lemenand, T., Ramadan, M., Khaled, M. (2020). Review on photovoltaic/thermal hybrid solar collectors: Classifications, applications and new systems. *Solar Energy, 207,* 1321–1347. DOI 10.1016/j.solener.2020.07.062.
4. Tschopp, D., Tian, Z., Berberich, M., Fan, J., Perers, B. et al. (2020). Large-scale solar thermal systems in leading countries: A review and comparative study of Denmark, China, Germany and Austria. *Applied Energy, 270,* 114997. DOI 10.1016/j.apenergy.2020.114997.
5. Gorjian, S., Ebadi, H., Calise, E., Shukla, A., Ingrao, C. (2020). A review on recent advancements in performance enhancement techniques for low-temperature solar collectors. *Energy Conversion and Management, 222,* 113246. DOI 10.1016/j.enconman.2020.113246.
6. Gao, D., Gao, G., Cao, J., Zhong, S., Ren, X. et al. (2020). Experimental and numerical analysis of an efficiently optimized evacuated flat plate solar collector under medium temperature. *Applied Energy, 269(3),* 115129. DOI 10.1016/j.apenergy.2020.115129.
7. Ahmadlouydarab, M., Ebadolahzadeh, M., Muhammad Ali, H. (2020). Effects of utilizing nanofluid as working fluid in a lab-scale designed FPSC to improve thermal absorption and efficiency. *Physica A: Statistical Mechanics and its Applications, 540(3),* 123109. DOI 10.1016/j.physa.2019.123109.
8. Wang, T. Y., Zhao, Y. H., Diao, Y. H., Ren, R. Y., Wang, Z. Y. (2019). Performance of a new type of solar air collector with transparent-vacuum glass tube based on micro-heat pipe arrays. *Energy, 177(142),* 16–28. DOI 10.1016/j.energy.2019.04.059.
9. Rubbi, F., Das, L., Habib, K., Aslfattahi, N., Saidur, R. et al. (2021). State-of-the-art review on water-based nanofluids for low temperature solar thermal collector application. *Solar Energy Materials and Solar Cells, 230(4),* 111220. DOI 10.1016/j.solmat.2021.111220.
10. Jang, S. P., Choi, S. U. (2006). Cooling performance of a microchannel heat sink with nanofluids. *Applied Thermal Engineering, 26(17–18),* 2457–2463. DOI 10.1016/j.applthermaleng.2006.02.036.

11. Awais, M., Bhuiyan, A. A., Salehin, S., Ehsan, M. M., Khan, B. et al. (2021). Synthesis, heat transport mechanisms and thermophysical properties of nanofluids: A critical overview. *International Journal of Thermofluids, 10(4),* 100086. DOI 10.1016/j.ijft.2021.100086.
12. Azam, A., Xu, T., Khan, M. (2020). Numerical simulation for variable thermal properties and heat source/sink in flow of cross nanofluid over a moving cylinder. *International Communications in Heat and Mass Transfer, 118(2),* 104832. DOI 10.1016/j.icheatmasstransfer.2020.104832.
13. Zaydan, M., Riahi, M., MEbarek-Oudina, F., Sehaqui, R. (2021). Mixed convection in a two—Sided lid-driven cavity filled with different types of nanoparticles: A comparative study assuming nanoparticles with different shapes. *Fluid Dynamics & Material Processing, 17(4),* 789–819. DOI 10.32604/fdmp.2021.015422.
14. Zeghbid, I., Bessaih, R. (2017). Mixed convection in a lid-driven cavity with heat sources using nanofluid. *Fluid Dynamics & Material Processing, 13(4),* 251–273. DOI 10.3970/fdmp.2017.013.251.
15. Jalali, H., Abbassi, H. (2020). Analysis of the influence of viscosity and thermal conductivity on heat transfer by Al_2O_3-water nanofluid. *Fluid Dynamics & Material Processing, 16(2),* 181–198. DOI 10.32604/fdmp.2020.07804.
16. Azam, M., Shakoor, A., Rasool, H. F., Khan, M. (2019). Numerical simulation for solar energy aspects on unsteady convective flow of MHD Cross nanofluid: A revised approach. *International Journal of Heat and Mass Transfer, 131(3),* 495–505. DOI 10.1016/j.ijheatmasstransfer.2018.11.022.
17. Azam, M., Mabood, F., Xu, T., Waly, M., Tlili, I. (2020). Entropy optimized radiative heat transportation in axisymmetric flow of Williamson nanofluid with activation energy. *Results in Physics, 19(3),* 103576. DOI 10.1016/j.rinp.2020.103576.
18. Mamedov, D., You, C. C., Karazhanov, S. Z., Marstein, E. S. (2019). Influence of si-nanoparticles on PEDOT: PSS properties for hybrid solar cells. *Materials Today: Proceedings, 33,* 2517–2519. DOI 10.1016/j.matpr.2020.04.906.
19. Rabbi, H. M. E., Sahin, A. Z., Yilbas, B. S., Al-Sharafi, A. (2021). Methods for the determination of nanofluid optical properties: A review. *International Journal of Thermophysics, 42(1),* 9. DOI 10.1007/s10765-020-02762-0.
20. Cuce, E., Cuce, P. M., Guclu, T., Besir, A. B. (2020). On the use of nanofluids in solar energy applications. *Journal of Thermal Science, 29(3),* 513–534. DOI 10.1007/s11630-020-1269-3.
21. Wahab, A., Hassan, A., Qasim, M. A., Ali, H. M., Babar, H. et al. (2019). Solar energy systems—Potential of nanofluids. *Journal of Molecular Liquids, 289(2),* 111049. DOI 10.1016/j.molliq.2019.111049.
22. Alexandrov, A., Zvaigzne, M., Lypenko, D., Nabiev, I., Samokhvalov, P. (2020). Al-, Ga-, Mg-, or Li-doped zinc oxide nanoparticles as electron transport layers for quantum dot light-emitting diodes. *Scientific Reports, 10(1),* 7496. DOI 10.1038/s41598-020-64263-2.
23. Zitoune, M., Ourrad Meziani, Q., Meziani, B., Adnani, M. (2016). Cooling of electronic components using nanofluid. *Fluid Dynamics & Materials Processing, 12(1),* 33–55. DOI 10.3970/fdmp.2016.012.033.
24. Al-Hassani, K. A., Alam, M. S., Rahman, M. M. (2021). Numerical simulations of hydromagnetic mixed convection flow of nanofluids inside a triangular cavity on the basis of a two-component nonhomogeneous mathematical model. *Fluid Dynamics & Materials Processing, 17(1),* 1–20. DOI 10.32604/fdmp.2021.013497.
25. Boungiorno, J., Hu, L. W., Kim, S. J., Hannink, R., Truong, B. et al. (2008). Nanofluids for enhanced economics and safety of nuclear reactors: An evaluation of the potential features issues, and research gaps. *Nuclear Technology, 162(1),* 80–91. DOI 10.13182/NT08-A3934.
26. Mahapatra, O., Bhagat, M., Gopalakrishnan, C., Arunachalam, K. D. (2008). Ultrafine dispersed CuO nanoparticles and their antibacterial activity. *Journal of Experimental Nanoscience, 3(3),* 185–193. DOI 10.1080/17458080802395460.
27. Singh, R., Lillard, J. W. Jr (2009). Nanoparticle-based targeted drug delivery. *Experimental and Molecular Pathology, 86(3),* 215–223. DOI 10.1016/j.yexmp.2008.12.004.
28. Azam, M., Xu, T., Shakoor, A., Khan, M. (2020). Effects of Arrhenius activation energy in development of covalent bonding in axisymmetric flow of radiative-cross nanofluid. *International Communications in Heat and Mass Transfer, 113(3),* 104547. DOI 10.1016/j.icheatmasstransfer.2020.104547.

29. Sajid, M. U., Bicer, Y. (2020). Nanofluids as solar spectrum splitters: A critical review. *Solar Energy, 207,* 974–1001. DOI 10.1016/j.solener.2020.07.009.
30. Liu, S., Afan, H. A., Aldlemy, M. S., Al-Ansari, N., Yaseen, Z. M. (2020). Energy analysis using carbon and metallic oxides-based nanomaterials inside a solar collector. *Energy Reports, 6,* 1373–1381. DOI 10.1016/j.egyr.2020.05.015.
31. Ghalandari, M., Maleki, A., Haghighi, A., Safdari Shadloo, M., Alhuyi Nazari, M. et al. (2020). Applications of nanofluids containing carbon nanotubes in solar energy systems: A review. *Journal of Molecular Liquids, 313(1),* 113476. DOI 10.1016/j.molliq.2020.113476.
32. Chen, M., He, Y., Zhu, J., Kim, D. R. (2016). Enhancement of photo-thermal conversion using gold nanofluids with different particle sizes. *Energy Conversion and Management, 112(13),* 21–30. DOI 10.1016/j.enconman.2016.01.009.
33. Nomoev, S., Adam, P. M., Bardakhanov, S., Vasilevskii, I., Movsesyan, A. et al. (2020). A visible light scattering study of silicon nanoparticles created in various ways. *Paper presented at the AIP Conference Proceedings, 2288,* 0028254. DOI 10.1063/5.0028254.
34. Xuan, Y., Duan, H., Li, Q. (2014). Enhancement of solar energy absorption using a plasmonic nanofluid based on TiO_2/Ag composite nanoparticles. *RSC Advances, 4(31),* 16206–16213. DOI 10.1039/C4RA00630E.
35. Chen, M., He, Y., Huang, J., Zhu, J. (2017). Investigation into au nanofluids for solar photothermal conversion. *International Journal of Heat and Mass Transfer, 108(15),* 1894–1900. DOI 10.1016/j.ijheatmasstransfer.2017.01.005.
36. Beicker, C. L. L., Amjad, M., Bandarra Filho, E. P., Wen, D. (2018). Experimental study of photothermal conversion using gold/water and MWCNT/water nanofluids. *Solar Energy Materials and Solar Cells, 188(3),* 51–65. DOI 10.1016/j.solmat.2018.08.013.
37. Ahmad, S. H. A., Saidur, R., Mahbubul, I. M., Al-Sulaiman, F. A. (2017). Optical properties of various nanofluids used in solar collector: A review. *Renewable and Sustainable Energy Reviews, 73,* 1014–1030. DOI 10.1016/j.rser.2017.01.173.
38. Said, Z., Saidur, R., Rahim, N. A. (2014). Optical properties of metal oxides based nanofluids. *International Communications in Heat and Mass Transfer, 59(1),* 46–54. DOI 10.1016/j.icheatmasstransfer.2014.10.010.
39. Sharaf, O. Z., Al-Khateeb, A. N., Kyritsis, D. C., Abu-Nada, E. (2018). Direct absorption solar collector (DASC) modeling and simulation using a novel Eulerian–Lagrangian hybrid approach: Optical, thermal, and hydrodynamic interactions. *Applied Energy, 231(3),* 1132–1145. DOI 10.1016/j.apenergy.2018.09.191.
40. Taylor, R. A., Phelan, P. E., Otanicar, T. P., Adrian, R., Prasher, R. (2011). Nanofluid optical property characterization: Towards efficient direct absorption solar collectors. *Nanoscale Research Letters, 6(1),* 225. DOI 10.1186/1556-276X-6-225.
41. Hota, S. K., Diaz, G. (2019). Activated carbon dispersion as absorber for solar water evaporation: A parametric analysis. *Solar Energy, 184(2),* 40–51. DOI 10.1016/j.solener.2019.03.080.
42. Bårdsgård, R., Kuzmenkov, D. M., Kosinski, P., Balakin, B. V. (2020). Eulerian CFD model of direct absorption solar collector with nanofluid. *Journal of Renewable and Sustainable Energy, 12(3),* 5144737. DOI 10.1063/1.5144737.
43. Song, D., Hatami, M., Wang, Y., Jing, D., Yang, Y. (2016). Prediction of hydrodynamic and optical properties of TiO_2/water suspension considering particle size distribution. *International Journal of Heat and Mass Transfer, 92(4),* 864–876. DOI 10.1016/j.ijheatmasstransfer.2015.08.101.
44. Hale, G. M., Querry, M. R. (1973). Optical constants of water in the 200-nm to 200-μm wavelength region. *Applied Optics, 12(3),* 555–563. DOI 10.1364/AO.12.000555.
45. Ermolaev, G. A., Tsapenko, A. P., Volkov, V. S., Anisimov, A. S., Gladush, Y. G. et al. (2020). Express determination of thickness and dielectric function of single-walled carbon nanotube films. *Applied Physics Letters, 116(23),* 231103. DOI 10.1063/5.0012933.
46. Bohren, C. F., Huffman, D. R. (1983). *Absorption and Scattering of Light by Small Particles*. Pennsylvania: Wiley.
47. Zeng, J., Xuan, Y. (2021). Analysis on interaction among solar light and suspended nanoparticles in nanofluids. *Journal of Quantitative Spectroscopy and Radiative Transfer, 269,* 107692. DOI 10.1016/j.jqsrt.2021.107692.

48. Research and Production Enterprise "Nanotechnology Center" (2021). Multi-walled carbon nanotubes DEALTOM. http://dealtom.ru/content/production.
49. Karcher (2021). Foamstop neutral, 125 ml. https://www.kaercher.com/int/home-garden/cleaning-and-care-agents/home-garden/vacuum-cleaner-with-water-filter-steam-vacuum-cleaner/foamstop/foamstop-neutral-62958730.html.
50. Agilent (2021). Advanced optical analysis with cary spectrophotometers for US-Vis spectroscopy & UV-Vis_NIR. https://www.agilent.com/en/products/uv-vis-uv-vis-nir/uv-vis-uv-vis-nir-systems/cary-100-uv-vis.
51. Scientific and Technical Company Soltec (2021). Ultrasonic baths Sapphire. https://stc-soltec.ru/oborudovanie/ultrazvukovye-vanny/ultrazvukovye-vanny-sapfir/.
52. Malvern Panalytical (2021). Zetasizer nano range–Support. https://www.malvernpanalytical.com/en/support/product-support/zetasizer-range/zetasizer-nano-range.
53. Ulset, E. T., Kosinski, P., Zabednova, Y., Zhdaneev, O. V., Struchalin, P. G. et al. (2018). Photothermal boiling in aqueous nanofluids. *Nano Energy, 50,* 339–346. DOI 10.1016/j.nanoen.2018.05.050.
54. Esmaeilzadeh, P., Hosseinpour, N., Bahramian, A., Fakhroueian, Z., Arya, S. (2014). Effect of ZrO_2 nanoparticles on the interfacial behavior of surfactant solutions at air-water and n-heptane-water interfaces. *Fluid Phase Equilibria, 361,* 289–295. DOI 10.1016/j.fluid.2013.11.014.
55. Gimeno-Furio, A., Hernandez, L., Barison, S., Agresti, F., Cabaleiro, D. et al. (2019). Optical characterization of oxidised carbon nanohorn nanofluids for direct solar energy absorption application. *Solar Energy, 191,* 323–331. DOI 10.1016/j.solener.2019.09.012.
56. Lee, S. H., Jang, S. P. (2013). Extinction coefficient of aqueous nanofluids containing multi-walled carbon nanotubes. *International Journal of Heat and Mass Transfer, 67,* 930–935. DOI 10.1016/j.ijheatmasstransfer.2013.08.094.
57. Lee, S. H., Jang, S. P. (2015). Efficiency of a volumetric receiver using aqueous suspensions of multi-walled carbon nanotubes for absorbing solar thermal energy. *International Journal of Heat and Mass Transfer, 80,* 58–71. DOI 10.1016/j.ijheatmasstransfer.2014.08.091.
58. Chen, W., Zou, C., Li, X. (2019). Application of large-scale prepared MWCNTs nanofluids in solar energy system as volumetric solar absorber. *Solar Energy Materials and Solar Cells, 200,* 109931. DOI 10.1016/j.solmat.2019.109931.
59. Jing, D., Song, D. (2017). Optical properties of nanofluids considering particle size distribution: Experimental and theoretical investigations. *Renewable and Sustainable Energy Reviews, 78(12),* 452–465. DOI 10.1016/j.rser.2017.04.084.